THE ASTROPHYSICAL JOURNAL, 442:177–185, 1995 March 20

OBSERVATIONS OF MAGNETIC FIELDS IN DIFFUSE CLOUDS

P. C. MYERS[1] AND A. A. GOODMAN[2]
Harvard-Smithsonian Center for Astrophysics, 60 Garden Street, Cambridge, MA 02138
R. GÜSTEN
Max-Planck-Institut für Radioastronomie, Auf dem Hügel 69, 53121 Bonn, Germany;
@ibm.rhrz.uni-bonn.de:p212gue@mpifr-bonn.mpg.de
AND
C. HEILES
Astronomy Department, University of California, Berkeley, CA 97420;
heiles@bkyast.berkeley.edu
Received 1994 April 8; accepted 1994 September 26

ABSTRACT

We report 32 statistically significant measurements of the line-of-sight component of the magnetic field strength, B_z, in four diffuse clouds, via the Zeeman effect in the 21 cm line of H I. The region near MBM 27–30 in the Ursa Major complex has $B_z > 4$ μG throughout a filamentary region 15 pc long, with significant structure on scales as small as 1.6 pc. The greatest field strength measured in this cloud is 19 ± 2 μG, greater than in most diffuse clouds by a factor ~ 2. Comparison of measurements with different telescopes suggests that the field strength at the map peak may be significantly greater than 19 μG on scales smaller than 1.6 pc. The magnetic and kinetic energy densities **M** and **K** in this cloud are comparable, within a factor 2 of 2×10^{-11} ergs cm^{-3}, and greater than the gravitational energy density by a factor ~ 500. Among the four clouds surveyed, six positions where CO emission is a local maximum have essentially the same mean line-of-sight field strength, $B_z \approx 8$ μG, as do four positions where CO emission is too weak to be detected The similarity of **M** and **K** in the diffuse clouds discussed here, as well as in denser, self-gravitating clouds, suggests strong coupling between magnetic fields and gas motions in some interstellar clouds, independent of their self-gravity. This coupling probably arises from ion-neutral collisions, which allow propagation of MHD waves.

Subject headings: ISM: clouds — ISM: magnetic fields — MHD — radio lines: ISM

1. INTRODUCTION

1.1. *Diffuse Clouds*

Diffuse interstellar clouds provide much of our information about the low-density interstellar medium. Their structure is complex, with evidence for sheets, filaments, and many size scales (e.g., Heithausen & Thaddeus 1990). They have too little mass to gravitationally bind the motions evident in their line widths (Heiles 1988; Magnani, Blitz, & Mundy 1985, hereafter MBM), although in some cases they may be stabilized by the pressure of the intercloud gas (Keto & Myers 1986). Their mean visual extinction generally lies in the range 0.1–1 mag. They have condensations which resemble the "cores" in darker clouds (Turner, Xu, & Rickard 1992), but if these condensations form stars they do so with much lower efficiency than do the cores in darker clouds (Magnani, Caillault, & Armus 1990; Kun 1992). We classify them here in terms of two of their defining properties—their emission in the 21 cm line of H I ("H I diffuse clouds") and in the 2.6 mm line of CO ("CO diffuse clouds").

The H I diffuse clouds are local maxima of H I line emission. They have visual extinction 0.1–0.3 mag. They are evident in the H I line and in the 60 and 100 μm emission characteristic of "infrared cirrus" (Low et al. 1984). They are not evident on the Palomar Sky Atlas prints and are generally not detected in the CO line, or are detected only in a region limited to a few arcmin (Heiles, Reach, & Koo 1988, hereafter HRK; Blitz, Bazell, and Désert 1990, hereafter BBD). Their fraction of molecular hydrogen is less than 0.01, according to observations of H and H_2 ultraviolet line absorption (Savage et al. 1977). However, their *IRAS* emission suggests that some low-extinction clouds have more H_2 than H I, even where CO is not detected (HRK; BBD).

The CO diffuse clouds include many "high-latitude molecular" clouds known by their faint absorption and/or reflection on the Palomar prints, their angular distance from the Galactic plane, and by their emission in the 2.6 mm $J = 1$–0 line of CO (MBM). Their visual extinction is generally 0.3–1 mag, greater than that of the H I diffuse clouds. They also include some clouds defined by their optical and ultraviolet absorption lines against background OB stars, such as ζ Oph (e.g., van Dishoeck & Black 1988). Their emission at 100 μm exceeds that expected from the grains associated with atomic H (de Vries, Heithausen, & Thaddeus 1987, hereafter VHT; HRK; BBD). The abundance of CO in high-extinction diffuse clouds increases significantly from low to high galactic latitude, perhaps because of differences in their ambient ultraviolet radiation field (Lada & Blitz 1988; Blitz 1991).

The foregoing characteristics of H I and CO diffuse clouds are sometimes seen in neighboring parts of the same region. Regions of CO emission generally have more extended H I emission at similar radial velocity (Gir, Blitz, & Magnani 1994), although bright, spatially well-defined regions of H I emission are only infrequently detected in the CO line (Lada, Dame, & Myers 1994).

1.2. *Magnetic Fields*

The magnetic and kinetic energy densities are comparable in many H I diffuse clouds (Heiles 1989; Verschuur 1989; § 3 of

[1] myers@cfa.harvard.edu.
[2] Also at Astronomy Department, University of California, Berkeley; agoodman@cfa.harvard.edu.

this paper). However, in CO diffuse clouds the ratio of magnetic and kinetic energies is less clear than in the H I diffuse clouds. Emission from many molecular lines has been detected in diffuse clouds, including the 18 cm OH lines (Magnani & Siskind 1990). But this emission is too weak to allow detection of the Zeeman effect.

In this paper we present a survey for the H I Zeeman effect in diffuse clouds which are bright in the 21 cm H I line, and which are known to have either extended CO emission, or sensitive upper limits on their CO emission. A related study of the H I Zeeman effect in the Ophiuchus molecular cloud complex is presented by Goodman & Heiles (1994).

Our main conclusion is that clouds with detected H I *and* CO emission generally have line-of-sight component of magnetic field strength $|B_z| = 5$–10 μG, essentially the same as do clouds with H I emission and undetected CO emission. In one cloud in Ursa Major, with both CO and H I emission, the line-of-sight component of the field is remarkably strong, with $|B_z| = 19$ μG in the strongest position, and extended, with $|B_z|$ more than 4 μG over 15 pc. A detailed comparison indicates that in this cloud, as in others with weaker fields, the magnetic energy density lies within a factor of 2 of the kinetic energy density, while each is greater than the gravitational energy density by more than an order of magnitude.

2. OBSERVATIONS

2.1. *Observational Procedure*

H I observations were made in 1990, 1991, and 1992 with the 26 m diameter telescope of the Hat Creek Radio Observatory (HCRO) of the University of California, Berkeley. The FWHM angular resolution was 36′. The intensity scale has about 20% uncertainty. The dual-channel cooled FET receiver provided an overall system temperature on cold sky of $\sim$45 K. The 1024 channel autocorrelator was split into two independent 512 channel banks, simultaneously observing opposite circular polarizations. The sense of polarization was switched at 100 s intervals by a motorized waveguide switch, to obtain the Stokes V spectrum. The total bandwidth was 625 kHz (132 km s^{-1}). After Hanning-smoothing, the velocity resolution was 0.52 km s^{-1}. The frequency of the local oscillator was switched electronically by 625 kHz, to obtain the Stokes I spectrum. Integration time on one position took 3–10 hr. Further observational details are given in Heiles (1988, 1989).

The H I spectra were analyzed by fitting the V profile to the frequency derivative of the I profile. Since the I profiles were usually simple and single-peaked, it was not necessary to do multicomponent Gaussian fits as described in Heiles (1989) and Goodman & Heiles (1994). Comparison of the multicomponent and single-component procedure gave values for B_z which generally differ by less than the 1 σ uncertainty in B_z, determined from the single-component fit.

In order to study the Ursa Major diffuse cloud in finer detail, H I mapping and Zeeman observations were undertaken with the 100 m telescope of the Max-Planck-Institut für Radioastronomie, in Effelsberg, Germany, in 1991 October and 1992 November. The telescope was equipped with a dual-channel, prime-focus receiver, with cooled HEMT amplifier, having overall zenith system temperature 25–30 K. The autocorrelator was split into two 512 channel sections, each 390 kHz wide, recording the left- and right-circularly polarized signals simultaneously. The data were frequency-switched by 1 MHz every second to obtain the Stokes I spectrum. The right- and left-circularly polarized spectra were differenced to obtain the Stokes V spectrum.

We checked the consistency of the two telescopes in their Zeeman effect response to a point source by observing the H I absorption features toward Cas A. The HCRO and 100 m telescopes give respectively 8.2 ± 0.7 and 14 ± 3 μG for the -48 km s^{-1} feature; and 20.0 ± 0.9 and 19 ± 3 μG for the -38 km s^{-1} feature. The marginally significant difference between these results is attributable to the relatively larger contribution from H I emission to the larger HCRO beam. These results are also consistent with the field strengths reported by Verschuur (1969) using the 43 m telescope of the National Radio Astronomy Observatory. Thus the HCRO and 100 m telescopes and their associated electronics and software have essentially the same Zeeman response to the field strengths of this order, when they originate in a region of small extent compared to either beam.

"Beam squint," or the displacement on the sky of the right- and left-circularly polarized beams of the telescope, can give rise to a spurious Zeeman effect if the observed line has a velocity gradient along the direction of squint, and if the combination of gradient and squint are sufficiently large. For the HCRO telescope, the magnitude $\theta_{\rm squint}$ of the beam squint is probably smaller than 1.′5 (Troland & Heiles 1982). We estimate the maximum possible magnitude of the fake magnetic field $B_{\rm squint}$ due to beam squint at $(l, b) = (141.1, 38.8)$, where the largest field strength was derived from the observations. We estimate this spurious field by assuming that $\theta_{\rm squint}$ has its maximum value of 1.′5, and that the squint direction is aligned precisely with the direction of the maximum velocity gradient G consistent with the observations. To determine this maximum gradient we examined the H I line center velocities at the nine positions observed nearest to (141.1, 38.8), and obtained $G = 3.2$ km s^{-1} deg^{-1} between (141.1, 38.8) and (140.9, 30.8). Then we can write

$$B_{\rm squint} = G f_0 \theta_{\rm squint}/cb = 2.3 \ \mu\text{G} ,$$

where f_0 is the rest frequency of the H I line (1420 MHz), c is the speed of light, and b is the g-factor of the H I transition (2.8 Hz μG^{-1}). This maximum value of $B_{\rm squint}$, 2.3 μG, is only slightly greater than the typical 1 σ value of B_z due to instrumental noise and is much smaller than the field strength, $B_z = 18.9$ μG observed at (141.1, 38.3). Thus beam squint cannot account for the observed field strength at this position, and similar estimates at other positions in the HCRO map lead to the same conclusion for all of the statistically significant field strengths in the map.

For the 100 m telescope, the altitude-azimuth mounting of the telescope implies that the sidelobe structure should rotate with hour angle, so that any beam squint effects should modulate the true Zeeman signal. However, no such modulation was evident above the noise in the observed data.

2.2. *Survey of* H I *Regions with Strong or Weak* CO *Emission*

The 10 regions listed in Table 1 were selected to be observed for the H I Zeeman effect by requiring that their H I line emission have peak line brightness temperature greater than 10 K, and that their CO line intensity be either "strong," brighter than 1 K and extended over greater than 10′ (Draco, VHT CO1, HMV 7, HMV 13, MBM 30, and MBM 27), or not extended, and fainter than about 0.5 K (VHT H1, VHT H2, dG1, dG2). The H I and CO line emission intensities were determined from reports of observations in Draco (Goerigk et

TABLE 1

HCRO OBSERVATIONS OF THE H I ZEEMAN EFFECT IN DIFFUSE H I AND CO CLOUDS

Cloud	l	b	T_B (K)	v_{LSR} (km s^{-1})	Δv (km s^{-1})	B_z (μG)	σ_{B_z} (μG)
A. CO Peaks							
Draco	89°.68	38°.41	6.5	−23.6	4.6	(11.1)	4.9
HMV 7	126.65	32.50	19.9	2.7	7.8	(7.1)	2.4
MBM 27	141.36	34.45	13.3	2.2	5.3	8.1	1.8
MBM 30	142.10	38.30	24.6	2.8	7.0	15.6	1.4
VHT CO1	143.00	38.60	23.1	3.7	7.8	5.0	1.3
HMV 13	146.85	40.66	17.3	1.9	8.9	6.3	2.1
Mean	...	...	19.6	...	7.3	8.8	1.7
B. CO Not Detected							
VHT HI1	141°.30	39°.30	21.6	5.9	11.2	10.0	1.8
VHT HI2	145.20	41.20	23.3	4.1	7.1	4.7	1.3
dG 1	348.26	24.17	43.4	−0.4	11.6	5.1	1.1
dG 2	349.47	17.07	61.1	3.6	11.0	(−1.7)	1.0
Mean	...	...	29.4	...	10.2	6.6	1.4

NOTE.—Values in parentheses of the line-of-sight component of the field strength, B_z, have signal-to-noise ratio $|B_z|/\sigma_{B_z} < 3$, and are considered statistically insignificant. The mean values are evaluated only for data with $B_z|/\sigma_{B_z} \geq 3$.

al. 1983; Mebold et al. 1985), in Ursa Major (VHT; MBM; Heithausen, Mebold, & de Vries 1987), and in Ophiuchus (de Geus 1988).

The results of the observations and analysis for the 10 surveyed positions are given in Table 1. These results show no significant difference in field strength B_z between the groups of positions (*a*) which are local maxima of extended CO emission, and (*b*) where CO was not detected. The ratio of mean values is 1.3, with 1 σ uncertainty 0.4. The samples are too small for a detailed statistical comparison, but they suggest that there is no dramatic variation in field strength, by a factor greater than 2, between the diffuse clouds with and without CO emission. The field strengths in each group lie within the same range 3–12 μG of the 44 statistically significant measurements in bright H I shells (Heiles 1989), with the exception of position (141.1, 38.8), discussed below.

The three greatest strengths in Table 1 were measured in the same region, the Ursa Major complex, which includes positions MBM 27, MBM 30, VHT CO1, VHT HI1, and VHT HI2. The largest of these, 18.9 ± 1.8 μG at position (141.1, 38.8) near VHT HI1, is remarkably strong for a diffuse cloud. Its Stokes I and V spectra are shown in Figure 1.

2.3. *Ursa Major Maps*

Large-scale mapping observations of the Stokes I and V spectra in Ursa Major were made with the HCRO telescope in 1991 and 1992, using the same observing and analysis procedures as described earlier. The sampling was on an irregular grid, following approximately the contours of H I and CO line brightness, with nearest neighbor spacing about one FWHM beamwidth, or 1.6 pc at the adopted distance of 150 pc, based on the optical extinction study by Penprase (1992). The approximate dimensions of the mapped region are 1.5 × 6 deg, or 4 × 16 pc. The positions and results are presented in Table 2, using the same format as in Table 1, and as contour maps of B_z in Figure 2*a* and of peak intensity T_A in Figure 2*b*. For completeness the four relevant entries from Table 1 are repeated in Table 2.

Table 2 and Figures 2*a* and 2*b* show that the line-of-sight component of the magnetic field in the Ursa Major complex has statistically significant values ($B_z/3\sigma_{B_z} > 3$) in the range 5–19 μG in 23 out of 37 observed positions. The line-of-sight field has significant detections over a projected extent 15 pc, and has coherent structure, which follows approximately the H I line brightness. The finest scale structure is that of the beam spacing, or about 1.6 pc.

The H I peak intensity maps with resolution 36′ (Fig. 2*b*) and 9′ (Fig. 2*c*) have the same general structure: an elongated feature extending from b = 38°.5 to 42°.5 at nearly constant l = 142° (hereafter, the "long filament"), and a less elongated feature (hereafter, the "short filament") extending from (l, b) = (142, 38.5) to (141, 39.8), making an angle of ~45° with the axis of the long filament. The map is brightest where the two features join, at (142.7, 38.4), the "bright spot." The long filament is narrower in the higher resolution map than in the lower resolution map. The peak intensity maps in Figures 2*b* and 2*c* have slightly more contrast and definition than do integrated intensity maps of the same spectra (not shown). The

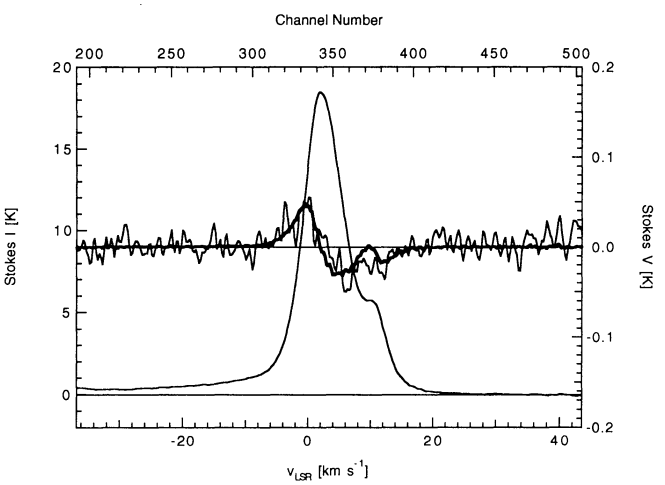

FIG. 1.—Stokes I and V spectra of the 21 cm H I line observed with the HCRO 26 m telescope toward position (l, b) = (141.1, 38.8), where the line-of-sight component of the magnetic field strength has its maximum value in the HCRO map, 18.9 ± 1.8 μG. The heavy line is the derivative of the I spectrum which best fits the V spectrum.

TABLE 2

HCRO MAPPING OBSERVATIONS OF THE H I ZEEMAN EFFECT IN THE URSA MAJOR DIFFUSE CLOUD COMPLEX

COORDINATES		T_B	v_{LSR}	Δv	B_z	σ_{B_z}	
l	b	(K)	(km s^{-1})	(km s^{-1})	(μG)	(μG)	ALIAS
140°.0	39°.0.....	5.8	3.5	12.7	(−1.7)	3.1	
140.0	39.7.....	12.7	3.2	9.2	5.7	1.5	
140.0	40.3.....	16.3	4.3	9.6	(1.7)	1.2	
140.5	38.0.....	8.0	3.0	7.7	(0.9)	2.3	
140.5	38.6.....	7.1	3.1	10.3	(3.8)	1.9	
140.5	39.2.....	12.3	3.7	12.0	7.2	1.9	
140.5	39.6.....	22.2	4.6	9.8	9.0	1.3	
140.5	40.3.....	17.1	5.5	10.6	(1.2)	1.8	
140.8	34.8.....	8.9	1.7	5.9	7.9	2.0	
140.9	38.3.....	9.7	2.9	7.2	(1.3)	1.5	
140.9	39.8.....	23.9	6.0	9.9	(−4.0)	2.0	
141.1	38.8.....	16.8	2.7	8.9	18.9	1.6	
141.3	34.2.....	8.1	2.0	6.2	12.6	1.6	
141.3	35.3.....	11.6	1.9	5.8	6.7	1.5	
141.3	39.3.....	21.6	5.9	11.2	10.0	1.8	VHT HI1
141.4	34.5.....	13.2	2.2	5.3	8.1	1.8	MBM 27
141.4	38.0.....	16.7	2.7	6.0	4.7	1.3	
141.5	36.0.....	10.2	1.7	6.8	5.5	1.7	
141.5	36.8.....	8.8	2.9	6.9	(1.8)	1.7	
141.5	37.3.....	10.1	3.4	8.0	(−5.2)	2.0	
141.9	35.3.....	14.1	2.4	5.1	11.0	1.4	
141.9	38.8.....	26.1	3.9	8.3	10.0	1.3	
142.1	34.8.....	8.4	2.0	6.7	11.1	1.7	
142.1	37.6.....	17.7	2.9	6.8	5.7	1.3	
142.1	38.3.....	24.6	2.8	7.0	15.6	1.4	MBM 30
142.1	39.5.....	18.0	6.2	11.3	(−2.4)	3.1	
142.3	36.0.....	14.8	2.8	5.4	(0.3)	1.3	
142.3	36.8.....	18.0	3.0	5.0	6.6	1.1	
142.6	35.3.....	10.5	2.5	6.5	6.5	1.5	
142.9	36.8.....	9.0	3.2	7.2	(3.5)	1.5	
142.9	37.6.....	15.7	3.4	9.0	8.0	2.0	
143.0	38.2.....	23.7	2.8	7.1	8.2	1.0	
143.0	38.6.....	23.1	3.7	7.8	5.0	1.3	VHT CO1
143.9	37.5.....	11.2	3.2	11.0	13.2	2.0	
144.0	37.2.....	9.6	3.5	12.3	(0.2)	4.1	
144.0	38.2.....	15.4	3.5	10.0	7.8	2.0	
144.9	38.0.....	13.1	3.4	11.1	(4.0)	2.5	

NOTE.—Values in parentheses have $|B_z|/\sigma_{B_z} < 3$ as in Table 1.

entire H I structure appears to be attached to an extended shell visible in H I and in *IRAS* (Heiles 1989; Meyerdiercks, Heithausen, & Reif 1991).

Figure 2*d* shows the CO intensity map of VHT, made with nearly identical resolution (FWHM 8′.8) as the H I map (9′.0) in Figure 2*c*. The peak positions of these two maps agree very closely in the long filament and in the bright spot, but the maps differ significantly north of the bright spot: the CO emission is strong to the northeast, where H I emission is absent; and the H I emission is strong in the short filament, to the northwest, where the CO emission is nearly absent. The CO emission profile is narrower than the H I profile across the long filament axis. In the short filament the CO emission is much weaker at the far end (141, 39.8) than at the near end (142, 38.5), while the H I intensity is more nearly uniform.

The map of the line-of-sight field strength, B_z, in Figure 2*a*, shows a closer correspondence to the H I intensity maps in Figures 2*b* and 2*c* than to the CO map in Figure 2*d*, but it does not match either map in detail. The region of strongest B_z is elongated and is similar to the region of brightest H I line intensity in extent, aspect ratio, and orientation. But the major axes of these two features are displaced by about 0°.5 along a perpendicular line, and the position of peak B_z is offset from the position of peak H I line brightness by 1°.6, or 2.7 beam FWHM. Along the major axis of strong B_z, B_z is poorly correlated with *IRAS* intensity, which probably traces total column density of H I and H_2, while along the long filament B_z appears to show a closer correspondence to the *IRAS* intensity, than to either the H I or CO intensity (Goodman et al. 1994).

2.4. *Zeeman Observations with the HCRO and 100 Meter Telescopes*

To select positions for Zeeman observation with the 100 m telescope it was first necessary to take into account the factor of 4 ratio of resolutions of the HCRO and 100 m telescopes. A preliminary map of H I spectra was made with 15′ spacing on a square grid in right ascension and declination, centered near the HCRO position of maximum field strength. This map is less extended than the more detailed map made later, and shown in Figure 2. These spectra show significant variation, with line intensity ranging over a factor of 2, line width ranging over a factor greater than 2, and line shape varying from symmetrical to double-peaked, on size scales as small as 15′, the map sampling interval.

Because of these differences in spectral profile from point to point within the HCRO beam area, three positions were selec-

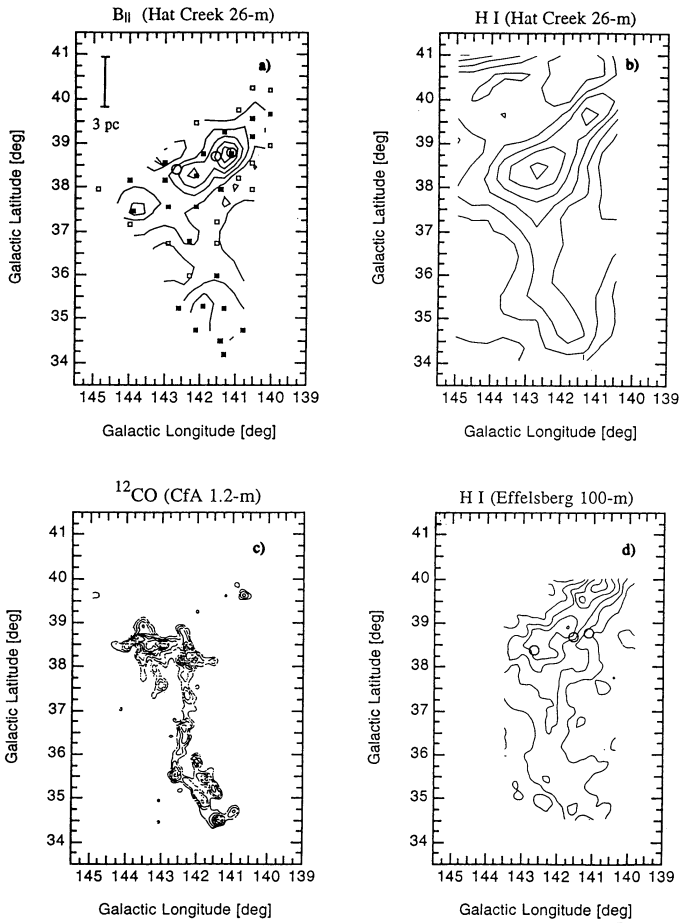

FIG. 2.—Structure of the line-of-sight magnetic field, atomic gas, and molecular gas in the Ursa Major complex. *Top left* (*a*): line-of-sight field strength, with minimum contour and contour interval 3 μG, determined from H I Zeeman observations with the HCRO. Positions marked with filled squares are detections, open squares are upper limits, contoured at 2 σ. Open circles indicate positions observed for the Zeeman effect with the 100 m telescope. *Top right* (*b*): peak temperature of H I emission, with minimum contour 6 K and interval 3 K, determined from H I observations with HCRO. *Bottom left* (*c*): integrated ^{12}CO line intensity, with minimum contour and contour interval 0.4 K km s^{-1}, measured by de Vries et al. (1987) with the 1.2 m telescope, now at the Harvard-Smithsonian Center for Astrophysics (CfA). *Bottom right* (*d*): Peak H I intensity, with minimum contour 0.20 of peak intensity, and contour interval 0.15 of peak intensity, measured at the 100 m telescope of the Max-Planck-Institut für Radioastronomie in Effelsberg, Germany. Open circles indicate positions observed for the Zeeman effect with the 100 m telescope.

ted for Zeeman measurements: (141.1, 38.8) because it is the position of maximum field strength in the HCRO map; (142.54, 38.715) because it has the simplest spectral profile among those near the (0, 0) position; and (142.66, 38.4) because it is the peak of the 100 m H I line intensity map. After a short period of integration at the (141.1, 38.8) position, it was clear that the Zeeman signature, if present, would be significantly weaker than that obtained at HCRO. Integration was therefore halted on this position in order to allow more time at the two other positions. The resulting line-of-sight field strengths and their 1 σ errors are 3.5 $\pm$ 3.7 μG at (141.1, 38.8); 11.4 $\pm$ 1.5 μG at (141.54, 38.715); and 11.1 $\pm$ 1.5 μG at (142.66, 38.4). These three positions are marked on the HCRO and 100 m maps in Figures 2*a* and 2*d*. Figure 3 shows the Stokes *I* and *V* spectra at (142.66, 38.4).

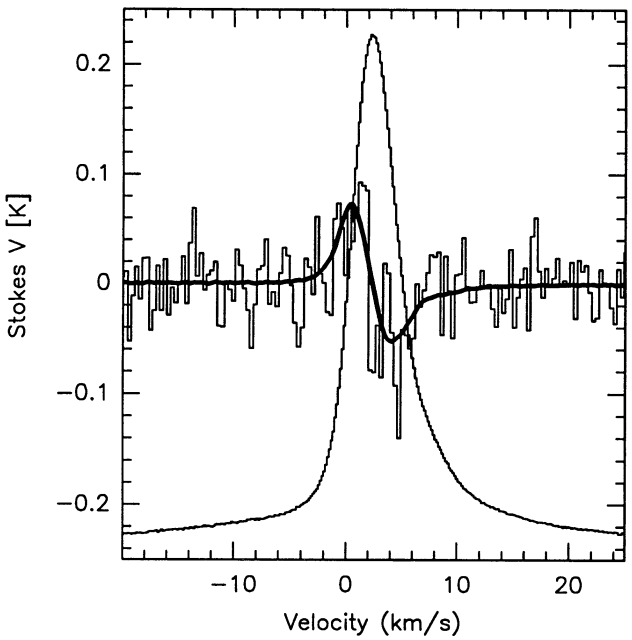

FIG. 3.—Stokes *I* and *V* spectra of the 21 cm H I cm line observed with the 100 m telescope of the MPIfR (FWHM beam = 9′) at position (*l*, *b*) = (142.66, 38.40), where the line-of-sight component of the magnetic field is 11.1 $\pm$ 1.5 μG. The heavy line is the derivative of the *I* spectrum which bests fits the *V* spectrum.

These three high-resolution (FWHM beam 9′) measurements of field strength appear mostly consistent with the HCRO measurements (36′) summarized in Table 2 and Figure 2*a*. At (141.54, 38.715), where the 100 m telescope measured 11.4 $\pm$ 1.5 μG, interpolation between data positions in the HCRO map in Figure 2*a* gives 12 μG, consistent within errors. At (142.66, 38.4) where the 100 m telescope measured 11.1 $\pm$ 1.5 μG, the HCRO maps give 9 μG, again consistent within errors. But at (141.1, 38.8) the HCRO field strength is 18.9 $\pm$ 1.8 μG, while the 100 m measurement is 3.5 $\pm$ 3.7 μG, essentially an upper limit. This apparent discrepancy, together with the other two nearby 100 m measurements, implies that we should find significant variation of field strength within the HCRO beam. In particular, if neither the HCRO nor the 100 m result at (141.1, 38.8) is spurious, then the 100 m should find $B_z > 18.9$ μG at some positions within the HCRO beam. This result also suggests that the field has significant structure on scales smaller than 1.6 pc. We look forward to these measurements in the future.

3. DISCUSSION

3.1. *Magnetic Fields in Diffuse Clouds*

The similarity of field strengths in diffuse clouds with and without extended CO emission, shown in Table 1, indicates that the expected increase in column density needed to shield CO from photodestruction, and the expected increase in number density needed to excite the $J = 1$–0 CO line, are not accompanied by a significant increase in field strength in the H I gas. The available data are too few to warrant a detailed model, but they favor a picture where the field strength in the atomic gas is relatively insensitive to conditions in the denser, molecular interior. This situation might arise in several ways, including (*a*) the field strength does not increase significantly

from the primarily atomic to the primarily molecular gas; or (*b*) the field strength increases from the atomic to the molecular gas, but the H I associated with the molecular gas is too small a component of the total H I gas to affect the observed Zeeman signal. Furthermore, the high or low intensity of CO emission need not always indicate high or low total gas density, as discussed in § 1 and in HRK.

3.2. *Energy Densities in the Ursa Major Complex*

The observations described in § 2 indicate that the magnetic field in the Ursa Major complex is remarkably strong for a diffuse cloud and that it is extended and coherent on a size scale of 15 pc, but with significant variation on scales as small as, or smaller than, 1.6 pc. In this section we estimate the total kinetic energy density **K**, the total magnetic energy density **M**, and the gravitational energy density **G** in the complex, to determine their relative values. Because the H I and CO maps have significant elongation we crudely model the cloud geometry in terms of cylinders to obtain the line-of-sight thickness Δz. We believe this is the most detailed comparison of energy densities which has been made for a diffuse interstellar cloud. We first evaluate the "partial" energy densities derived directly from observables: the kinetic energy density in the atomic gas, **K**(H I), and the magnetic energy density $\mathbf{M}_z$ corresponding to the line-of-sight component of the field strength, B_z.

We model the geometry of the complex as two axially symmetric cylinders in the plane of the sky, having partial overlap as illustrated in Figure 4. These cylinders correspond to the long and short filaments discussed in § 2.2. The long cylinder has a uniform envelope which is purely atomic, and a uniform core which is partly molecular and partly atomic. The core has width 0.87 pc, one-third that of the envelope, based on the CO map of VHT. The short cylinder is purely atomic, with the same constant density as the envelope of the long cylinder. The cylinders have length 8.0 and 12 pc, and common width 2.7 pc, based on the H I emission map in Figure 2*c*. The H I column density is thus uniform, except in the overlap region, defined to consist of positions (141.9, 38.8), (142.1, 38.3), (143.0, 38.2), and (143.0, 38.6). There the line-of-sight thickness is assumed to be 5.4 pc, twice the assumed thickness of the H I distribution at all other map positions. (An alternative geometry would have the two cylinders merge in three dimensions, rather than in projection as assumed here. If so, the column density in the overlap region would be unchanged, the density would increase by a factor of 2, and the thickness would decrease by a factor of 2).

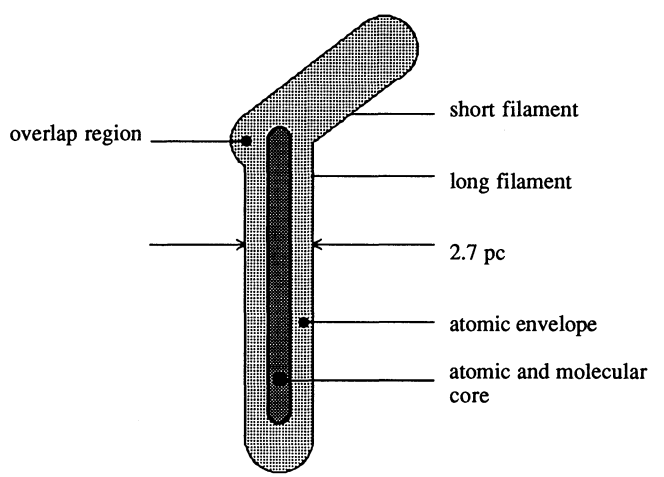

FIG. 4.—Schematic model of the Ursa Major diffuse cloud complex, used to evaluate energy densities.

For each position in Table 2, Table 3A lists column density N(H I), kinetic energy density **K**(H I), and the magnetic energy density $\mathbf{M}_z$ corresponding to the line-of-sight component of the magnetic field strength B_z.

The column density of H I is computed from

$$N(\text{H I}) = 1.823 \times 10^{18} (\pi/[4 \ln 2])^{1/2} T_B \Delta v \text{ cm}^{-2} , \quad (1)$$

where T_B is the peak line brightness temperature in K, Δv is the FWHM line width in km s^{-1}, and where the line shape is assumed to be Gaussian (e.g., Spitzer 1978, eq. [3-38]).

TABLE 3A

H I COLUMN DENSITIES AND PARTIAL KINETIC AND MAGNETIC ENERGY DENSITIES IN THE URSA MAJOR DIFFUSE CLOUD COMPLEX

COORDINATE		N(H I)	**K**(H I)	$\mathbf{M}_z$
l	b	(10^{20} cm^{-2})	(10^{-11} ergs cm^{-3})	
140°0	39°7.....	2.3	1.1	0.13
140.5	39.2.....	2.8	2.3	0.21
140.5	39.6.....	4.2	2.3	0.32
140.8	34.8.....	1.0	0.20	0.25
141.1	38.8.....	2.9	2.3	1.4
141.3	34.2.....	0.97	0.21	0.63
141.3	35.3.....	1.3	0.25	0.18
141.3	39.3.....	4.7	3.3	0.40
141.4	34.5.....	1.4	0.22	0.26
141.4	38.0.....	1.9	0.40	0.088
141.5	36.0.....	1.3	0.35	0.12
141.9	35.3.....	1.4	0.21	0.48
141.9	38.8.....	4.2	0.80	0.40
142.1	34.8.....	1.1	0.28	0.49
142.1	37.6.....	2.3	0.62	0.13
142.1	38.3.....	3.3	0.47	0.97
142.3	36.8.....	1.7	0.25	0.17
142.6	35.3.....	1.3	0.32	0.17
142.9	37.6.....	2.7	1.3	0.25
143.0	38.2.....	3.2	0.47	0.27
143.0	38.6.....	3.5	0.61	0.099
143.9	37.5.....	2.4	1.7	0.69
144.0	38.2.....	3.0	1.7	0.24
Mean.....		2.3	0.93	0.36

NOTE.—Column density, kinetic energy density, and magnetic energy density are given only for the 23 positions in Table 2 where the magnetic field strength was detected with $|B_z|/\sigma_{B_z} > 3$.

TABLE 3B

TOTAL ENERGY DENSITIES IN THE URSA MAJOR DIFFUSE CLOUD COMPLEX

K	**M**	**G**
1.3	2.2	0.038

NOTE.—Each energy density has units of 10^{-11} ergs cm^{-3} and estimated uncertainty of a factor of 2.

The kinetic energy density $\mathbf{K}$(H I) in the atomic gas at each position is computed from

$$\mathbf{K}(\text{H I}) = 3mn\sigma^2/2 = 1.5 \times 10^{-33} N(\text{H I})(\Delta z)^{-1} \Delta v^2 \text{ ergs cm}^{-3}, \quad (2)$$

where m is the mass per H atom, n is the mean number density, σ is the one-dimensional velocity dispersion, equal to $\Delta v/(8 \ln 2)^{1/2}$, and Δz is the line-of-sight extent of the gas, in pc. The kinetic energy density is dominated by nonthermal motions, since the thermal component of Δv at 100 K is only about 2 km s^{-1}, while the mean observed value of Δv in Table 2 is 8 km s^{-1}. We use the values of Δv from Table 2, N(H I) from Table 3A, and $\Delta z = 2.7$ or 5.4 pc as estimated above. This estimate assumes that all of the H I gas along a line of sight through the cloud has the observed line width and does not account for possible H I line width differences in the core and envelope portions of the line of sight.

The magnetic energy density in the line-of-sight component of the field is computed from $\mathbf{M}_z = B_z^2/8\pi$, using values of B_z from Table 2. The values of $\mathbf{K}$(H I) range from 0.2 to 3.3×10^{-12} ergs cm^{-3}, and the values of $\mathbf{M}_z$ range from 0.087 to 1.4×10^{-12} ergs cm^{-3}. The values of $\mathbf{K}$(H I) and $\mathbf{M}_z$ show no detailed correlation. The mean values $\langle N(\text{H I})\rangle$, $\langle \mathbf{K}(\text{H I})\rangle$, and $\langle \mathbf{M}_z\rangle$ in the last row of Table 3A are unweighted averages over the individual measurements.

Table 3B presents estimated values of the total kinetic, magnetic, and gravitational energy densities in the Ursa Major cloud. The total kinetic energy density in the envelope $\mathbf{K}_{\text{env}}$ equals 1.4 times $\langle \mathbf{K}(\text{H I})\rangle$ from Table 3A, accounting for 10% He by number. The kinetic energy density in the core part of the model cloud was estimated, based on the CO line width and the density of H_2 obtained from the visual extinction. However, the core volume occupies too small a fraction ($\frac{1}{9}$) of the total volume of the long cylinder to make a significant change in the total kinetic energy density $\mathbf{K}$. Thus $\mathbf{K} \approx \mathbf{K}_{\text{env}} = 1.4\langle \mathbf{K}(\text{H I})\rangle$.

The total magnetic energy density $\mathbf{M}$ is estimated to be greater than $\langle M_z\rangle$ from Table 3A by a factor 6 by assuming that $\langle B^2\rangle = 3\langle B_z^2\rangle$ (McKee et al. 1993) and that the total magnetic field energy density, including the nonuniform component, is greater than that of the uniform component by a factor of 2. A factor of order 2 is suggested by the variation between high-resolution and low-resolution observations at (141.1, 38.8) discussed earlier, and by the analysis of optical polarization by Jones, Dickey, & Klebe (1992) and by Myers & Goodman 1991).

The gravitational energy density $\mathbf{G}$ is expressed in terms of $\mathbf{G}_{\text{sphere}}$, the gravitational energy density of a uniform sphere, by

$$\mathbf{G} = f\mathbf{G}_{\text{sphere}} = f(\pi G/5)(3mN/2)^2, \quad (3)$$

with gravitational constant G and with mass column density mN equal to the mean column density of the cloud, 1.4 $m_{\text{H}}\langle N(\text{H I})\rangle$. Here m_{H} is the proton mass. The correction to $\mathbf{G}_{\text{sphere}}$ because of the elongated shape of the cloud is $f = 1.5$ for the aspect ratio 4.5 of the longer cylinder and $f = 1.3$ for the aspect ratio 2.9 of the shorter cylinder, using equation (B3) of Bertoldi & McKee (1992). We adopt $f = 1.4$. These corrections are small compared to the difference between $\mathbf{G}$ (3.8×10^{-14} ergs cm^{-3}) and the other energy densities ($\mathbf{K} = 1.3 \times 10^{-11}$ ergs cm^{-3} and $\mathbf{M} = 2.2 \times 10^{-11}$ ergs cm^{-3}). The uncertainty in each energy density, due mainly to the uncertainty in cloud dimensions and the idealized nature of the model, is estimated to be a factor of about 2.

The magnetic field strength in the Ursa Major cloud is unusually high for a diffuse cloud, but the foregoing estimates indicate that the magnetic energy density is not much greater than the kinetic energy density: the two are comparable because the velocity dispersions and densities in the Ursa Major cloud are also greater than average for diffuse clouds. In contrast, the kinetic and magnetic energy densities are each greater than the gravitational energy density by a factor of ~ 500.

3.3. *Energy Densities in Diffuse* H I *Clouds*

Zeeman measurements by Heiles (1989) indicate 44 H I features yielding reliable, statistically significant values of B_z, out of 73 positions bright in H I "shells." Among these, the column density of H I is 0.7–8 $\times 10^{20}$ cm^{-2}, with typical value 2×10^{20} cm^{-2}. Most of these positions appear dominated by atomic, rather than molecular, gas (Lada et al. 1994). The mean line-of-sight component of field strength is $|B_z| = 6$ μG. For this value, we estimate the total magnetic energy density $\mathbf{M} = 6|B_z|^2/8\pi$, on the same basis as in § 3.2 above, to be 1×10^{-11} ergs cm^{-3}, or half the value in the Ursa Major cloud.

In the H I shell clouds of Heiles (1989), the kinetic energy density $\mathbf{K}$ spans a wider range than does $\mathbf{M}$, since the values of N(H I), Δz, and Δv each vary by a factor of 2–3. We adopt N(H I) $= 2 \times 10^{20}$ cm^{-2} and $\Delta v = 6$ km s^{-1}, mean values from Heiles (1989), and $\Delta z = 1$–3 pc, taking into account the relatively small scale filamentary structure of the H I emission indicated by the maps of Joncas, Boulanger, & Falgarone (1992) and by Heithausen (1987). Then $\mathbf{K} = 4 \times 10^{-12}$ ergs cm^{-3} to 1×10^{-11} ergs cm^{-3}, yielding $\mathbf{M}/\mathbf{K} = 1$–3. This ratio indicates that the magnetic and kinetic energy densities are comparable in many H I diffuse clouds.

Thus the Ursa Major diffuse cloud complex, with substantial CO and H I emission, has about the same relation of energy densities as a large number of diffuse H I clouds lacking CO emission: the kinetic and magnetic energy densities are comparable within a factor of order 2. In contrast, the gravitational energy density in Ursa Major and in other diffuse clouds is negligibly small compared to the kinetic and magnetic energy densities.

3.4. *Energy Densities in Molecular Clouds*

In more than 100 molecular clouds with greater densities than the diffuse clouds studied here, the gravitational and kinetic energy densities are known to be comparable (Larson 1981); and in all of the 15 clouds with sufficient available information, the gravitational, kinetic, *and* magnetic energy densities are comparable (Myers & Goodman 1988). Thus wherever kinetic energy densities have been compared to magnetic energy densities derived from Zeeman observations, the two energy densities appear comparable, independent of whether the cloud is self-gravitating.

On the other hand, many searches for the Zeeman effect in molecular clouds have been negative as is also the case for diffuse clouds. Eleven of the 12 dark clouds searched for the Zeeman effect by Crutcher et al. (1993) were negative: the mean 3 σ line-of-sight field strength $|B_z|_{\text{max}}$ was 10 μG, and the field strength needed for equal magnetiic and kinetic energy densities was greater than $|B_z|_{\text{max}}$ by a mean factor 2.6. Evidently regions with the greatest field strengths are easiest to detect, have $\mathbf{M} \approx \mathbf{K}$, and represent the maximum observable coupling

between the magnetic field and the gas motions. Considering those regions with $\mathbf{M} \approx \mathbf{K}$, it is clear that some have $\mathbf{K} \gg \mathbf{G}$ (diffuse clouds) while others have $\mathbf{K} \approx \mathbf{G}$ (denser molecular clouds).

A similar conclusion comes from the line widths studied by Fuller & Myers (1993, hereafter FM) in thermally dominated, self-gravitating dense cores. There it is necessary to distinguish the thermal and nonthermal components of the kinetic energy density $\mathbf{K} = \mathbf{K}_T + \mathbf{K}_{NT}$ since $\mathbf{K}_{NT} \ll \mathbf{K}_T \approx \mathbf{K}$ in thermal cores (FM), whereas in diffuse clouds $\mathbf{K}_T \ll \mathbf{K}_{NT} \approx \mathbf{K}$ (e.g., Heiles 1989). In both thermal cores and diffuse clouds the nonthermal kinetic energy density $\mathbf{K}_{NT}$ is not strongly coupled to the gravitational energy density $\mathbf{G}$, since $\mathbf{K}_{NT}/\mathbf{G} \approx 0.1$ in thermal cores and $\mathbf{K}_{NT}/\mathbf{G} > 10$ in diffuse clouds. Yet in thermal cores as in diffuse clouds $\mathbf{K}_{NT}/\mathbf{M}$ is probably closer to unity than is $\mathbf{K}_{NT}/\mathbf{G}$. For estimation of $\mathbf{K}_{NT}/\mathbf{M}$ we adopt density 1×10^4 cm^{-3} and nonthermal velocity dispersion 0.07 km s^{-1}, typical of the values found by FM, and field strength bounded by the mean galactic field ~ 5 μG (Rand & Kulkarni 1989), and upper limits in more extended clouds, ~ 16 μG (Crutcher et al. 1993). Then $\mathbf{K}_{NT}/\mathbf{M}$ ranges from 0.4 to 4, while $\mathbf{K}_{NT}/\mathbf{G}$ for the nine starless cores studied by FM has mean $\pm$ standard error 0.10 ± 0.03, assuming typical column density of 5×10^{21} cm^{-2}.

The results reported here, together with those discussed above, suggest that the coupling between the magnetic field and the gas motions responsible for the similar values of $\mathbf{K}_{NT}$ and $\mathbf{M}$ in some interstellar clouds is independent of gravity, and applies to clouds with a wide range of $\mathbf{K}_{NT}/\mathbf{G}$: to thermal cores with $\mathbf{K}_{NT}/\mathbf{G} \ll 1$, molecular clouds with $\mathbf{K}_{NT}/\mathbf{G} \sim 1$, and diffuse clouds with $\mathbf{K}_{NT}/\mathbf{G} \gg 1$. We caution that this conclusion applies only to clouds with measured field strengths. Those clouds with measured upper limits, and other clouds which have not been observed, may or may not have energetically significant magnetic fields.

3.5. *Physical Basis of the Coupling between Magnetic and Kinetic Energy*

The similarity of $\mathbf{K}_{NT}$ (or $\mathbf{K}$) and $\mathbf{M}$ in clouds with detections of the Zeeman effect implies that the magnetic and kinetic energies are well coupled, but does not by itself clarify the physical basis of the coupling. The leading candidate for this coupling is collisions between the neutral molecules, primarily H_2, and the ions tied to the magnetic field lines. If the collisions occur rapidly enough, magnetohydrodynamic (MHD) waves can propagate in the field-fluid system at the Alfvén speed of the neutral plus ions, rather than in the field alone, at the Alfvén speed of the ions (e.g., Kulsrud & Pearce 1969; Arons & Max 1974; Zweibel & Josafatsson 1983; McKee et al. 1993). If the magnetic energy in the waves is similar to the energy in the mean magnetic field, the observed nonthermal line widths should approximate the Alfvén speed in the neutrals plus ions. Equivalently, the nonthermal kinetic energy density $\mathbf{K}_{NT}$ should approximate the magnetic energy density $\mathbf{M}$.

Thus two conditions should be satisfied to yield energetically significant MHD waves in the neutral gas: (1) the ion fraction, due primarily to ionization by UV photons and cosmic rays, should be high enough to allow propagation of MHD waves in the field-fluid system; and (2) the rate of wave excitation should exceed the rate of wave dissipation. These points will be explored in more detail in future publications.

4. SUMMARY

The main points presented in this paper are as follows.

1. Ten diffuse cloud regions bright in the 21 cm H I line were surveyed for the Zeeman effect—six regions which are local maxima of emission in the CO $J = 1$–0 line and four regions where no CO could be detected. The two groups have no significant difference in mean detected field strength, each about 8 μG. The kinetic and magnetic energy densities appear comparable in each group, within a factor 2 of 1×10^{-11} ergs cm^{-3}.

2. A diffuse cloud in Ursa Major with both CO and H I emission has maximum line-of-sight field strength 19 ± 2 μG. The field strength was detected with significance greater than 3 σ in 23 of 37 positions in this cloud. It has large-scale structure over about 15 pc, but also varies on scales as small as, or smaller than, 1.6 pc. The magnetic, kinetic, and gravitational energy densities are evaluated in detail. The magnetic and kinetic energy densities are each within a factor 2 of 2×10^{-11} ergs cm^{-3}, while the gravitational energy density is smaller by a factor of about 500.

3. The similarity of kinetic and magnetic energy densities in these clouds, as well as in those denser, self-gravitating "dark" and "molecular" clouds where the field strength has been measured, suggests that kinetic and magnetic energy are closely coupled in some interstellar clouds, independent of whether the clouds are close to equilibrium between gravity and nonthermal motions. The coupling probably arises from ion-neutral collisions, which allow the propagation of magnetohydrodynamic waves in the combined field-gas system.

We thank the staffs of the HCRO and of the MPIfR for their assistance with observations. We thank A. Heithausen for kindly communicating unpublished data. We thank C. McKee, E. Zweibel, and V. Khersonsky for helpful discussions.

REFERENCES

Arons, J., & Max, C. E. 1975, ApJ, 196, L77
Bally, J., Langer, W., Stark, A., & Wilson, R. 1987, ApJ, 312, L45
Bertoldi, F., & McKee, C. F. 1992, ApJ, 395, 135
Blitz, L. 1991, in Molecular Clouds, ed. R. A. James & T. J. Millar (Cambridge: Cambridge Univ. Press), 49
Blitz, L., Bazell, D., & Désert, F. X. 1990, ApJ, 352, L13 (BBD)
Bohlin, R. C., Savage, B. D., & Drake, J. F. 1978, ApJ, 224, 132
Crutcher, R. M., Troland, T. H., Goodman, A. A., Heiles, C., Kazès, I., & Myers, P. C. 1993, ApJ, 407, 175
de Geus, E. 1988, Ph.D. thesis, Univ. Leiden
de Vries, H. W., Heithausen, A., & Thaddeus, P. 1987, ApJ, 319, 723 (VHT)
Elmegreen, B. G. 1990, ApJ, 361, L77
Falgarone, E., & Puget, J.-L. 1986, A&A, 162, 235
Fuller, G. A., & Myers, P. C. 1993, ApJ, 418, 273 (FM)
Gir, B.-Y., Blita, L., & Magnani, L. 1994, ApJ, in press
Goerigk, W., Mebold, U., Reif, K., Kalberla, P. M. W., & Velden, L. 1983, A&A, 120, 63
Goodman, A. A., Bastien, P., Myers, P. C., & Ménard, F. 1990, ApJ, 359, 363
Goodman, A. A., Crutcher, R. M., Heiles, C., Myers, P. C., & Troland, T. H. 1989, ApJ, 338, L61
Goodman, A. A., & Heiles, C. 1994, ApJ, 424, 208
Goodman, A. A., Myers, P. C., Güsten, R., & Heiles, C. 1994, in The First Symposium on the Infrared Cirrus and Diffuse Interstellar Clouds, ed. W. Latter & R. Cutri (ASP Conf. Ser.), in press
Heiles, C. 1987, in Physical Processes in Interstellar Clouds, ed. G. E. Morfill & M. Scholer (Dordrecht: Reidel), 429
———. 1988, ApJ, 324, 321
———. 1989, ApJ, 336, 808

Heiles, C., Reach, W. T., & Koo, B.-C. 1988, ApJ, 322, 313 (HRK)
Heithausen, A. 1987, Ph.D. thesis, Rheinischen Friedrich-Wilhelms-Universität, Bonn
Heithausen, A., Mebold, U., & de Vries, H. W. 1987, A&A 179, 263
Heithausen, A., & Thaddeus, P. 1990, ApJ, 306, L109
Joncas, G., Boulanger, F., & Falgarone, E. 1992, ApJ, 397, 165
Jones, T. J., Dickey, J. M., & Klebe, D. 1992, ApJ, 389, 602
Keto, E. R., & Myers, P. C. 1986, ApJ, 304, 466
Kulsrud, R. M., & Pearce, W. P. 1969, ApJ, 156, 445
Kun, M. 1992, A&AS, 92, 875
Lada, E. A., & Blitz, L. 1988, ApJ, 326, L69
Lada, E. A., Dame, T. M., & Myers, P. C. 1994, in preparation
Larson, R. B. 1981, MNRAS, 194, 809
Loren, R. B. 1989, ApJ, 338, 902
Low, F. J., et al. 1984, ApJ, 278, L19
Magnani, L. 1987, Ph.D. thesis, Univ. Maryland
Magnani, L., Blitz, L., & Mundy, L. 1985, ApJ, 295, 402 (MBM)
Magnani, L., Caillault, J.-P., & Armus, L. 1990, ApJ, 357, 602
Magnani, L., & Siskind, L. 1990, ApJ, 359, 355
Mebold, U., Cernicharo, J., Velden, L., Reif, K., Crezelius, C., & Goerigk, W. 1985, A&A, 151, 427
McKee, C. F., Zweibel, E. G., Goodman, A. A., & Heiles, C. 1993, in Protostars and Planets III, ed. E. Levy & J. Lunine (Tucson: Univ. Arizona Press), 327
Meyerdierks, H., Heithausen, A., & Reif, K. 1991, A&A, 245, 247
Mouschovias, T. Ch. 1976a, ApJ, 206, 753
———. 1976b, ApJ, 207, 141
Myers, P. C., & Goodman, A. A. 1988, ApJ, 326, L27
———. 1991, ApJ, 373, 509
Myers, P. C., Fuller, G. A., Goodman, A. A., & Benson, P. J. 1991, ApJ, 376, 561
Penprase, B. E. 1992, ApJS, 83, 273
Rand, R. J., & Kulkarni, S. 1989, ApJ, 343, 760
Savage, B. D., Bohlin, R. C., Drake, J. F., & Budich, W. 1977, ApJ, 216, 291
Shu, F., & Terebey, S. 1984, in Cool Stars, Stellar Systems, and the Sun, ed. S. Baliunas & L. Hartmann (Lecture Notes in Phys., 193), 78
Spitzer, L. 1978, Physical Processes in the Interstellar Medium (New York: Wiley)
Troland, T. H. 1990, in Galactic and Intergalactic Magnetic Fields, ed. R. Beck, P. P. Kronberg, & R. Wielebinski (Dordrecht: Kluwer), 293
Troland, T. H., & Heiles, C. 1982, ApJ, 252, 179
Turner, B. E., Xu, L.-P., & Rickard, L. J. 1992, ApJ, 391, 158
van Dishoeck, E. F., & Black, J. H. 1988, ApJ, 334, 771
Verschuur, G. L. 1989, ApJ, 339, 163
Zweibel, E., & Josafattson, K. 1983, ApJ, 270, 511